Effective field theory interactions for liquid argon target in DarkSide-50 experiment

P. Agnes,[1] I.F.M. Albuquerque,[2] T. Alexander,[3] A.K. Alton,[4] M. Ave,[2] H.O. Back,[3] G. Batignani,[5, 6] K. Biery,[7] V. Bocci,[8] G. Bonfini,[9] W.M. Bonivento,[10] B. Bottino,[11, 12] S. Bussino,[13, 14] M. Cadeddu,[15, 10] M. Cadoni,[15, 10] F. Calaprice,[16] A. Caminata,[12] N. Canci,[1, 9] A. Candela,[9] M. Caravati,[15, 10] M. Cariello,[12] M. Carlini,[9, 17] M. Carpinelli,[18, 19] S. Catalanotti,[20, 21] V. Cataudella,[20, 21] P. Cavalcante,[22, 9] S. Cavuoti,[20, 21] A. Chepurnov,[23] C. Cicalò,[10] A.G. Cocco,[21] G. Covone,[20, 21] D. D'Angelo,[24, 25] S. Davini,[12] A. De Candia,[20, 21] S. De Cecco,[8, 26] M. De Deo,[9] G. De Filippis,[20, 21] G. De Rosa,[20, 21] A.V. Derbin,[27] A. Devoto,[15, 10] F. Di Eusanio,[16, 22] M. D'Incecco,[9] G. Di Pietro,[9, 25] C. Dionisi,[8, 26] M. Downing,[28] D. D'Urso,[18, 19] E. Edkins,[29] A. Empl,[1] G. Fiorillo,[20, 21] K. Fomenko,[30] D. Franco,[31] F. Gabriele,[9] C. Galbiati,[16, 17, 9, 32] C. Ghiano,[9] S. Giagu,[8, 26] C. Giganti,[33] G.K. Giovanetti,[16] O. Gorchakov,[30] A.M. Goretti,[9] F. Granato,[34] A. Grobov,[35, 36] M. Gromov,[23, 30] M. Guan,[37] Y. Guardincerri,[7, a] M. Gulino,[38, 19] B.R. Hackett,[29] K. Herner,[7] B. Hosseini,[10] D. Hughes,[16] P. Humble,[3] E.V. Hungerford,[1] Al. Ianni,[9] An. Ianni,[16, 9] V. Ippolito,[8] T.N. Johnson,[39] K. Keeter,[40] C.L. Kendziora,[7] I. Kochanek,[9] G. Koh,[16] D. Korablev,[30] G. Korga,[1, 9] A. Kubankin,[41] M. Kuss,[5] M. La Commara,[20, 21] M. Lai,[15, 10] X. Li,[16] M. Lissia,[10] G. Longo,[20, 21] A.A. Machado,[42] I.N. Machulin,[35, 36] A. Mandarano,[17, 9] L. Mapelli,[16, 10] S.M. Mari,[13, 14] J. Maricic,[29] C.J. Martoff,[34] A. Messina,[8, 26] P.D. Meyers,[16] R. Milincic,[29] A. Monte,[7, 28] M. Morrocchi,[5, 6] V.N. Muratova,[27] P. Musico,[12] A. Navrer Agasson,[33] A.O. Nozdrina,[35, 36] A. Oleinik,[41] M. Orsini,[9] F. Ortica,[43, 44] L. Pagani,[39] M. Pallavicini,[11, 12] L. Pandola,[19] E. Pantic,[39] E. Paoloni,[5, 6] K. Pelczar,[9, 45] N. Pelliccia,[43, 44] E. Picciau,[15, 10] A. Pocar,[28] S. Pordes,[7] S.S. Poudel,[1] H. Qian,[16] F. Ragusa,[24, 25] M. Razeti,[10] A. Razeto,[9] A.L. Renshaw,[1] M. Rescigno,[8] Q. Riffard,[31] A. Romani,[43, 44] B. Rossi,[21] N. Rossi,[8] D. Sablone,[16, 9] O. Samoylov,[30] W. Sands,[16] S. Sanfilippo,[14, 13] C. Savarese,[17, 9, 16] B. Schlitzer,[39] E. Segreto,[42] D.A. Semenov,[27] A. Shchagin,[41] A. Sheshukov,[30] P.N. Singh,[1] M.D. Skorokhvatov,[35, 36] O. Smirnov,[30] A. Sotnikov,[30] C. Stanford,[16] S. Stracka,[5] Y. Suvorov,[20, 21, 35] R. Tartaglia,[9] G. Testera,[12] A. Tonazzo,[31] P. Trinchese,[20, 21] E.V. Unzhakov,[27] M. Verducci,[8, 26] A. Vishneva,[30] R.B. Vogelaar,[22] M. Wada,[16, 10] T.J. Waldrop,[4] H. Wang,[46] Y. Wang,[46] A.W. Watson,[34] S. Westerdale,[16] M.M. Wojcik,[45] X. Xiang,[16] X. Xiao,[46] C. Yang,[37] Z. Ye,[1] C. Zhu,[16] and G. Zuzel[45]

(The DarkSide-50 Collaboration)

[1] *Department of Physics, University of Houston, Houston, TX 77204, USA*
[2] *Instituto de Física, Universidade de São Paulo, São Paulo 05508-090, Brazil*
[3] *Pacific Northwest National Laboratory, Richland, WA 99352, USA*
[4] *Physics Department, Augustana University, Sioux Falls, SD 57197, USA*
[5] *INFN Pisa, Pisa 56127, Italy*
[6] *Physics Department, Università degli Studi di Pisa, Pisa 56127, Italy*
[7] *Fermi National Accelerator Laboratory, Batavia, IL 60510, USA*
[8] *INFN Sezione di Roma, Roma 00185, Italy*
[9] *INFN Laboratori Nazionali del Gran Sasso, Assergi (AQ) 67100, Italy*
[10] *INFN Cagliari, Cagliari 09042, Italy*
[11] *Physics Department, Università degli Studi di Genova, Genova 16146, Italy*
[12] *INFN Genova, Genova 16146, Italy*
[13] *INFN Roma Tre, Roma 00146, Italy*
[14] *Mathematics and Physics Department, Università degli Studi Roma Tre, Roma 00146, Italy*
[15] *Physics Department, Università degli Studi di Cagliari, Cagliari 09042, Italy*
[16] *Physics Department, Princeton University, Princeton, NJ 08544, USA*
[17] *Gran Sasso Science Institute, L'Aquila 67100, Italy*
[18] *Chemistry and Pharmacy Department, Università degli Studi di Sassari, Sassari 07100, Italy*
[19] *INFN Laboratori Nazionali del Sud, Catania 95123, Italy*
[20] *Physics Department, Università degli Studi "Federico II" di Napoli, Napoli 80126, Italy*
[21] *INFN Napoli, Napoli 80126, Italy*
[22] *Virginia Tech, Blacksburg, VA 24061, USA*
[23] *Skobeltsyn Institute of Nuclear Physics, Lomonosov Moscow State University, Moscow 119234, Russia*
[24] *Physics Department, Università degli Studi di Milano, Milano 20133, Italy*
[25] *INFN Milano, Milano 20133, Italy*
[26] *Physics Department, Sapienza Università di Roma, Roma 00185, Italy*
[27] *Saint Petersburg Nuclear Physics Institute, Gatchina 188350, Russia*
[28] *Amherst Center for Fundamental Interactions and Physics Department, University of Massachusetts, Amherst, MA 01003, USA*
[29] *Department of Physics and Astronomy, University of Hawai'i, Honolulu, HI 96822, USA*
[30] *Joint Institute for Nuclear Research, Dubna 141980, Russia*

[31] APC, Université Paris Diderot, CNRS/IN2P3, CEA/Irfu, Obs de Paris, USPC, Paris 75205, France
[32] Museo della fisica e Centro studi e Ricerche Enrico Fermi, Roma 00184, Italy
[33] LPNHE, CNRS/IN2P3, Sorbonne Université, Université Paris Diderot, Paris 75252, France
[34] Physics Department, Temple University, Philadelphia, PA 19122, USA
[35] National Research Centre Kurchatov Institute, Moscow 123182, Russia
[36] National Research Nuclear University MEPhI, Moscow 115409, Russia
[37] Institute of High Energy Physics, Beijing 100049, China
[38] Engineering and Architecture Faculty, Università di Enna Kore, Enna 94100, Italy
[39] Department of Physics, University of California, Davis, CA 95616, USA
[40] School of Natural Sciences, Black Hills State University, Spearfish, SD 57799, USA
[41] Radiation Physics Laboratory, Belgorod National Research University, Belgorod 308007, Russia
[42] Physics Institute, Universidade Estadual de Campinas, Campinas 13083, Brazil
[43] Chemistry, Biology and Biotechnology Department, Università degli Studi di Perugia, Perugia 06123, Italy
[44] INFN Perugia, Perugia 06123, Italy
[45] M. Smoluchowski Institute of Physics, Jagiellonian University, 30-348 Krakow, Poland
[46] Physics and Astronomy Department, University of California, Los Angeles, CA 90095, USA

We reanalize data collected with the DarkSide-50 experiment and recently used to set limits on the spin-independent interaction rate of weakly interacting massive particles (WIMPs) on argon nuclei with an effective field theory framework. The dataset corresponds to a total (16660 ± 270) kg d exposure using a target of low-radioactivity argon extracted from underground sources. We obtain upper limits on the effective couplings of the 12 leading operators in the nonrelativistic systematic expansion. For each effective coupling we set constraints on WIMP-nucleon cross sections, setting upper limits between 2.4×10^{-45} cm^2 and 2.3×10^{-42} cm^2 (8.9×10^{-45} cm^2 and 6.0×10^{-42} cm^2) for WIMPs of mass of 100 GeV/c^2 (1000 GeV/c^2) at 90% confidence level.

PACS numbers: To be defined

INTRODUCTION

Astrophysical and cosmological observations show that most of the matter in the Universe is dark and nonbaryonic, whose intrinsic nature is still unknown [1–3]. Compelling theoretical models assume that dark matter consists of weakly interacting massive particles (WIMPs), a simple hypothesis able to explain the most crucial phenomenology [4] with relative ease, like rotation curves of spiral galaxies, the observations of anisotropies of the cosmic microwave background, gravitational lensing at galactic scale, and the big-bang nucleosynthesis. Present theoretical research describes the interaction between WIMPs and target nuclei in terms of effective field theory (EFT) operators [5–7]. The lowest-order term in a systematic nonrelativistic expansion is an interaction that does not depend on the relative velocity v of the incoming particle or on the momentum transfer $\vec{q}$, which can be parametrized by spin-independent (SI) and spin-dependent cross sections. The SI cross section is the only one relevant for spin-zero nuclei and, if WIMPs interact coherently with all nucleons, it is enhanced by a factor equal to the mass number A relative to incoherent cross sections like the spin-dependent cross section.

The standard SI WIMP-nucleus interaction in the galactic standard halo scenario [8–10] is the benchmark that is used to compare different experiments. The physical interpretation of the observed results changes under different hypotheses for the interaction. Such a consider-

ation is important given the present unclear experimental landscape. On the one hand, DAMA [12, 13] recorded a signal that is interpreted as collisions of WIMPs with mass of a few tens of GeV/c^2 and the CDMS II-Si [14] result appears to be better fitted by a model with WIMPs than by one with only reasonable backgrounds. On the other hand, the lack of signals in other experiments, such as Xenon100 [15], LUX [16], PANDAX-II [17], and XENON1T [18] seems to contradict the existence of WIMPs of this mass, if the SI interaction is coherent and independent of the nucleus [11]. WIMP-nucleus interactions that differ from the lowest-order SI one could alleviate the tension between experiments that use different target nuclei. In fact, cross sections from other operators can depend on characteristics of the target nuclei besides the mass number A. In particular, they can uniquely depend on the WIMP mass and velocity yielding interaction rates that span many orders of magnitude [19–24].

In this work, we briefly review the main ideas underlying a general classification of operators and form factors that can appear in WIMP-nucleus interactions. We then focus on an argon target and, specifically, to the DarkSide-50 dataset [25].

EFFECTIVE FIELD THEORY EXPANSION FOR LIQUID ARGON NUCLEI

Following the model independent approach to WIMP-nucleus scattering that uses a Galilean-invariant EFT

and the notation of Ref. [7], the interaction between two particles with nonzero masses can be reduced to a linear combination of 15 operators, if we assume, in analogy with the standard analysis for the SI interaction, that coupling coefficients c_i are equal for protons and neutrons (isospin independent interaction):

$$\mathcal{O}_{\rm int} \equiv \sum_{i=1}^{15} c_i \mathcal{O}_i \quad . \tag{1}$$

This assumption makes it possible to compare limits from experiments that use different target nuclei. Providing limits on specific dynamical WIMP interaction models or combining future positive WIMP signals from different target nuclei to gain information on the isospin content of the interaction requires twice as many operators and corresponding couplings.

Seven operators contribute to the nuclear matrix elements of the interaction of a WIMP with the spin-zero nucleus of ^{40}Ar:

$$\begin{aligned}
\mathcal{O}_1 &= 1_\chi 1_N \\
\mathcal{O}_3 &= i\vec{S}_N \cdot \left(\frac{\vec{q}}{m_N} \times \vec{v}^\perp \right) \\
\mathcal{O}_5 &= i\vec{S}_\chi \cdot \left(\frac{\vec{q}}{m_N} \times \vec{v}^\perp \right) \\
\mathcal{O}_8 &= \vec{S}_\chi \cdot \vec{v}^\perp \\
\mathcal{O}_{11} &= i\vec{S}_\chi \cdot \frac{\vec{q}}{m_N} \\
\mathcal{O}_{12} &= \vec{S}_\chi \cdot \left(\vec{S}_N \times \vec{v}^\perp \right) \\
\mathcal{O}_{15} &= - \left(\vec{S}_\chi \cdot \frac{\vec{q}}{m_N} \right) \left[\vec{S}_N \times \left(\vec{v}^\perp \right) \cdot \frac{\vec{q}}{m_N} \right] \quad , \tag{2}
\end{aligned}$$

where m_N is the nucleon mass, $\vec{S}_\chi$ and $\vec{S}_N$ are the WIMP and the nucleon spins, $\vec{q}$ is momentum transfer in the collision, and $\vec{v}^\perp \equiv \vec{v} - \vec{q}(\vec{v} \cdot \vec{q})/q^2 = \vec{v} + \vec{q}/(2\mu_T)$ is the transverse relative velocity. The last equality follows from energy conservation and $\mu_T \equiv (m_\chi m_T)/(m_\chi + m_T)$ is the reduced mass between a WIMP of mass m_χ and a target nucleus of mass m_T. Operators $\mathcal{O}_{12}$ and $\mathcal{O}_{15}$ can appear only for mediators with spin greater than one. Since the typical energy transfer in WIMP-nucleus collision is much lower than the nuclear binding energy, and the collision is essentially nonrelativistic, the differential elastic cross section can be naturally organized so that nuclear and particle physics factorize [7] as follows:

$$\begin{aligned}
\frac{d\sigma_N}{dE_R}(q, v) &= \frac{2m_T}{v^2} \sum_k R_k \left(\vec{v}_T^{\perp 2}, \frac{\vec{q}^2}{m_N^2} \right) W_k^{00}(\vec{q}^2) \tag{3} \\
&= \frac{2m_T W_M^{00}(0)}{v^2} \sum_k R_k \left(\vec{v}_T^{\perp 2}, \frac{\vec{q}^2}{m_N^2} \right) \frac{W_k^{00}(\vec{q}^2)}{W_M^{00}(0)}
\end{aligned}$$

where $E_R = \vec{q}^2/(2m_T)$ is the nucleus recoil energy, m_T is the mass of the target nucleus, the R_k's are the WIMP re-

sponse functions, which depend parametrically on the operator coupling coefficients $\{c_i\}$, and the W_k^{00} are the corresponding nuclear response functions. These response functions generalize the standard form factor, which reflects the finite size of the nucleus, by taking into account the velocities of the nucleons. The "00" superscript indicates the isoscalar-isoscalar combination, as in Ref. [7]. For spin-zero nuclei, three response functions appear, $k = M$, Φ'', or $M\Phi''$ using the notation of Ref. [7]. If only c_1, the coupling of the SI operator $\mathcal{O}_1$, is different from zero, then only $R_M = c_1^2$ appears. In this case Eq. (3) reduces to the standard SI result:

$$\frac{d\sigma_N}{dE_R}(q, v) = \frac{2m_T c_1^2}{v^2} W_M^{00}(\vec{q}^2) = \frac{A^2 \sigma_1}{\mu_N^2} \frac{m_T}{2v^2} \frac{W_M^{00}(\vec{q}^2)}{W_M^{00}(0)} , \tag{4}$$

where we have defined the WIMP-nucleon cross section

$$\sigma_1 \equiv c_1^2 \mu_N^2 \frac{4W_M^{00}(0)}{A^2} , \tag{5}$$

with μ_N the WIMP-nucleon reduced mass and A the mass number. The normalized response function, $W_M^{00}(\vec{q}^2)/W_M^{00}(0)$, corresponds to the square of the form factor that is often parametrized using the Helm form factor [8].

When a more general interaction is considered, the response functions R_k's can be dependent on the momentum transfer and on the relative velocity of the incoming particles. One can classify the various contributions to the differential cross section according to the powers of $\vec{q}^2 = 2m_T E_R$ and $\vec{v}^{\perp 2}$ that appear in the WIMP response functions R_k. Equations (37) and (38) in Ref. [7] show the contributions to the elastic differential cross section in Eq. (3). These contributions have the following powers of $\vec{q}^2$ and $\vec{v}^{\perp 2}$:

- the WIMP response function R_M^{00}, which multiples the nuclear response function W_M^{00}, has four terms, proportional to 1, $\vec{q}^2$, $\vec{v}^{\perp 2}$, and $\vec{q}^2 \cdot \vec{v}^{\perp 2}$;

- the WIMP response function $R_{\Phi''}^{00}$, which multiples the nuclear response function $W_{\Phi''}^{00}$, has three terms, proportional to $\vec{q}^2$, $\vec{q}^4$, and $\vec{q}^6$;

- finally, the WIMP response function $R_{M\Phi''}^{00}$, which multiples the nuclear response function $W_{M\Phi''}^{00}$, has two contributions proportional to $\vec{q}^2$, and $\vec{q}^4$.

Since in the kinematic regime of interest higher powers of $\vec{q}^2$ are expected to be subdominant, we choose to leave out the term proportional to $\vec{q}^6$. The EFT expansion in Eq. (4) is left with eight contributions that differ because they have different powers of $\vec{q}^2$ or $\vec{v}^{\perp 2}$ or different nuclear response functions.

If we include the possibility that the interaction mediator could be much lighter than the momentum transfer and, therefore, that the differential cross section could

contain an additional factor proportional to $(\Lambda/q)^4$ with Λ a momentum scale, we find eight additional possibilities for a total of 16 possible combinations of powers of $\vec{q}^{\,2}$ or $\vec{v}^{\perp 2}$ and nuclear responses. A similar classification of the possible interactions have been proposed in Ref. [26]. Reference [26], however, considers also terms proportional to $\vec{v}^{\perp 4}$, but such terms do not arise in EFT [see Eq. (38) in Ref. [7]], and does not take into account that additional operators could probe different form factors. Given a specific theoretical model, where the ratios between all the couplings c_i are given, we could make an exclusion curve as a function of an overall scale of the interaction. In the standard approach only c_1 is assumed different from zero. In the same spirit of probing a single coupling at the time, this work shows results for the cases when only one coefficient in the expansion in Eq. (1) is different from zero. Table I lists the 12 remaining terms of the expansion: the four terms that multiply the mixed nuclear response function $M\Phi''$ have not been considered, since they appear when at least two c_i are different from zero. Note that, in principle, the power-counting classification and the implied relative importance of the different contributions could be modified by QCD effects; see for instance the chiral EFT in Ref. [27], or by fine-tuning the c_i parameters of the nucleus-WIMP interaction. Each of the 12 terms of the EFT expansion leads to a term in the differential cross section

$$\frac{d\sigma_N}{dE_R}(q,v) = 2c_i^2 d_i \frac{m_T}{v^2}\left(\frac{q}{q_{\rm ref}}\right)^{2\alpha}\left(\frac{v^\perp}{v_{\rm ref}}\right)^{2\beta} W_k^{00}(\vec{q}^{\,2})\ (6)$$

$$= \frac{A^2\sigma_i}{\mu_N^2}\frac{m_T}{2v^2}\left(\frac{q}{q_{\rm ref}}\right)^{2\alpha}\left(\frac{v^\perp}{v_{\rm ref}}\right)^{2\beta}\frac{W_k^{00}(\vec{q}^{\,2})}{W_M^{00}(0)}(7)$$

where $\alpha = 0$, 1 or 2 and $\beta = 0$ or 1, d_i are dimensionless coefficients, which are explicitly given in the last column of Table I and k labels the nuclear response function. In analogy with Eqs. (4) and (5) we have also defined a cross section $\sigma_i \equiv c_i^2 d_i(\sigma_1/c_1^2)$ for each term and we have introduced $q_{\rm ref}$ and $v_{\rm ref}$, typical momentum transfer and velocity in a direct dark matter phenomenology so that σ_i has the dimension of a cross section. Specific theoretical models fix the values of $\sigma_i/(q_{\rm ref}^{2\alpha}v_{\rm ref}^{2\beta})$. A different choice would scale $\sigma_i \to \sigma_i(q'_{\rm ref}/q_{\rm ref})^{2\alpha}(v'_{\rm ref}/v_{\rm ref})^{2\beta}$. We present our results using $q_{\rm ref} = 100$ MeV/c and $v_{\rm ref} = v_0 = 220$ km/s, the standard halo local velocity. The nuclear response functions W_M^{00} and $W_{\Phi''}^{00}$ for ^{40}Ar have been taken from Ref. [28].

The total interaction rate R is obtained from Eq. (7) by integrating over the recoil energy E_R in the experimental window and over the WIMP velocities

$$R = N_T\frac{\rho}{m_\chi}\int dE_R\int d^3v\frac{d\sigma_N}{dE_R}(E_R,v)vf(v)\,,\quad (8)$$

where N_T is the number of target nuclei, $\rho = 0.3$ GeV/ (c^2 cm^3) is the local dark matter density, and $f(v)$ is a Maxwellian velocity distribution [8] with a cutoff $v_{\rm esc} =$

Operator Coupling	R_k Expansion	Nuclear Response	d_i
c_1^2	1	W_M^{00}	1
c_{11}^2	$\left(\frac{q}{q_{\rm ref}}\right)^2$	W_M^{00}	$\frac{j_\chi(j_\chi+1)}{3}\left(\frac{q_{\rm ref}}{m_N}\right)^2$
c_8^2	$\left(\frac{v^\perp}{v_{\rm ref}}\right)^2$	W_M^{00}	$\frac{j_\chi(j_\chi+1)}{3}v_{\rm ref}^2$
c_5^2	$\left(\frac{q}{q_{\rm ref}}\right)^2\left(\frac{v^\perp}{v_{\rm ref}}\right)^2$	W_M^{00}	$\frac{j_\chi(j_\chi+1)}{3}\left(\frac{q_{\rm ref}}{m_N}\right)^2 v_{\rm ref}^2$
c_{12}^2	$\left(\frac{q}{q_{\rm ref}}\right)^2$	$W_{\Phi''}^{00}$	$\frac{j_\chi(j_\chi+1)}{12}\left(\frac{q_{\rm ref}}{m_N}\right)^2$
c_3^2	$\left(\frac{q}{q_{\rm ref}}\right)^4$	$W_{\Phi''}^{00}$	$\frac{1}{4}\left(\frac{q_{\rm ref}}{m_N}\right)^4$
c_1^{*2}	$\left(\frac{q_{\rm ref}}{q}\right)^4$	W_M^{00}	
c_{11}^{*2}	$\left(\frac{q_{\rm ref}}{q}\right)^2$	W_M^{00}	
c_8^{*2}	$\left(\frac{q_{\rm ref}}{q}\right)^4\left(\frac{v^\perp}{v_{\rm ref}}\right)^2$	W_M^{00}	
c_5^{*2}	$\left(\frac{q_{\rm ref}}{q}\right)^2\left(\frac{v^\perp}{v_{\rm ref}}\right)^2$	W_M^{00}	
c_{12}^{*2}	$\left(\frac{q_{\rm ref}}{q}\right)^2$	$W_{\Phi''}^{00}$	
c_3^{*2}	1	$W_{\Phi''}^{00}$	

TABLE I. List of addition powers of q and $v^\perp$ relative to the SI scalar operator in the nonrelativistic EFT expansion in Eq. (1) of the differential cross section in Eq. (3), when only operators contributing to spin-zero nuclei are considered and only one of the couplings c_i in Eq. (1) is different from zero. The first column shows the c_i's, following the notation of Ref. [7], whereas the second column shows the corresponding powers of q and $v^\perp$ appearing in the WIMP response functions R_k and finally the third column lists the corresponding nuclear response functions associated to the operator. The fourth column shows the dimensionless coefficient d_i that appears in Eq. (6), where m_N is the nucleon mass, j_χ is the WIMP spin, and $v_{\rm ref}$ is relative to the speed of light. The star $*$ denotes cases with a light mediator with propagator $(\Lambda/q)^4$; the relations between the σ_i^*'s and c_i^* are the same as the case of the heavy mediator, but the c_i^* change with $q_{\rm ref}$ as $c_i^* = c_i(\Lambda/q_{\rm ref})^2$ given the operator combination of Eq. (1).

544 km/s [9, 10] and velocities $v_0 = 220$ km/s and $v_E = 232$ km/s [11].

Since the DarkSide-50 experiment has not detected any WIMP event, limits for each of the 12 cross sections σ_i are given as a function of the WIMP mass M_χ. Figure 1 shows the normalized shape of the recoil energy for five selected operators in an argon detector with the acceptance of DarkSide-50 [25]. The solid curve (number 3) corresponds to the standard SI operator. The other four curves are examples which give the most extreme results in terms of the final WIMP-nucleus cross-section exclusion limits for each of the two response functions Φ'' and M. Given enough WIMP events the recoil spectrum should make it possible to distinguish between different interaction models. A statistical analysis that takes into account the different expected recoil spectra gives stronger exclusion curves if background is present; this is not our case, since the DarkSide-50 experiment has a total expected background after the selection of

only about 0.1 events.

In the experimental realizations, the rate in Eq. (8) is convolved with detector resolution and the energy scale must be rescaled according to the relation

$$Q(E_R) = LY \times E_R \times \mathcal{L}_{\text{eff}}(E_R), \qquad (9)$$

where $Q(E_R)$ is the energy estimator, LY the light yield in photoelectrons (PEs) per keV and $\mathcal{L}_{\text{eff}}(E_R)$ is the nuclear-recoil quenching. In this new variable Eq. (3) becomes

$$\frac{d\sigma_N}{dE_R}(q, v) \to \frac{d\sigma_N}{dE_R}\frac{dE_R}{dQ} \otimes \mathcal{R}(Q), \qquad (10)$$

where $\mathcal{R}$ is the resolution function and $\otimes$ denotes the convolution product. The calibration of the energy scale for nuclear recoils and the experimental resolution are briefly described in the next section.

EFT LIMITS IN DARKSIDE-50 EXPERIMENT

The DarkSide-50 experiment, located at Laboratori Nazionali del Gran Sasso (LNGS), following the results of its predecessor DarkSide-10 [29], searches for nuclear recoils (NRs) induced by WIMP scattering with a liquid argon double-phase time projection chamber (LAr-TPC), surrounded by a spherical liquid scintillator veto (LSV) located in the center of a cylindrical water Cherenkov veto. The active veto detectors are used for rejecting the coincidences in the LAr-TPC induced by cosmic and material radiation (see, for details, [30, 31, 36–40]). Two arrays of 19 Photo Multipliers each of 3", facing from the top and the bottom the liquid argon active volume ($\sim$ 46.4 kg), detect the primary scintillation light (whose signal is called S1) and the gas scintillation from drifted ionization electrons (whose signal is called S2). LAr intrinsic scintillation characteristics allow us to reject electron recoils (ERs), essentially beta and gamma events from background, at the level of 1.5×10^7 or even better [36]. The particle identification is based on the fraction of S1 detected in the first 90 ns from the pulse start time (f_{90} parameter).

The DarkSide-50 experiment took data in two campaigns: first, the atmospheric argon campaign, in which the main features of the detector have been understood and tested [36]; second, the underground depleted argon (UAr) campaign in which the predicted characteristics have been confirmed and the impressive reduction of the ^{39}Ar isotope has been proven [31].

UAr was extracted in Colorado gas plants, purified at Fermilab and shipped to LNGS, during an intense cooperation of many years [41]. The ^{39}Ar activity of UAr is a factor $(1.4 \pm 0.2) \times 10^3$ lower than the atmospheric argon one, corresponding to an activity of (0.73 ± 0.11) mBq/kg [31].

The TPC response calibration is performed with neutron and gamma sources and with gaseous ^{83m}Kr injected into the target volume [32]. The S1 scintillation efficiency of nuclear recoils was measured with test beam experiments, namely SCENE [33] and ARIS [34], and cross-calibrated with AmBe and AmC neutron sources in DarkSide-50 [35]. The analysis uses both S1 and S2. S1 gives information on the nature of the event and is the main energy variable. However, a combination of S1 and S2 gives an energy variable with better resolution and linearity, since the deposited energy is shared between scintillation and ionization. In addition, S2 determines the position and rejects multiple scatter events. Reference [36] describes the procedure to calibrate the nuclear-recoil energy scale from the scintillation signal using the PE yield for nuclear recoils of known energy measured in the SCENE experiment [33]. In summary, SCENE measures the ratio between the PE yield from NR at 200 V/cm and that from ^{83m}Kr at zero field. The DarkSide-50 zero-field PE yield for ^{83m}Kr (8.0 ± 0.2 PE/keV [25] measured at the peak energy of 41.5 keV) then gives the NR PE yield vs. S1. We assume constant NR PE yield above the highest SCENE-measured energy, $\sim$ 57.3 keV$_{\text{nr}}$. Monte Carlo simulations estimate that the overall S1 light collection efficiency, averaged on the entire volume, is about $\sim$ 16%. The analysis of the DarkSide-50 data is performed in blind mode as explained in Ref. [25]. The expected background events can be classified into three categories: surface events, neutrons (cosmogenic and radiogenic), and ERs. Surface events are mostly rejected with fiducialization of the active volume, neutrons are efficiently suppressed with the LSV, and ERs are rejected with high efficiency using the f_{90} parameter. The LSV, whose estimated efficiency is 0.9964 ± 0.0004, identified 4 neutron candidates. After the LSV cut, the dominant background comes from ERs (0.08 ± 0.04 surviving events). The f_{90} acceptance requires a relatively large nuclear-recoil threshold energy. The final acceptance is 60.9%, with a threshold energy $\gtrsim$50 keV$_{\text{nr}}$ (see Fig. 10 of Ref. [25]) and the fiducial mass corresponds to 36.9 ± 0.6 kg. The number of expected surviving background events for the entire statistics, which corresponds to (16660 ± 270) kg d exposure, is 0.09 ± 0.04 (for a detailed summary see Table V of Ref. [25]). After the data unblinding, no events were observed in the defined WIMP search region, as shown in Fig. 11 (right) of Ref. [25]. The lack of observed events is consistent with up to 2.3 WIMP-nucleon scatters expected at 90% C.L. and so can be used to draw 90% C.L. exclusion curves for the σ_i cross sections in terms of the 12 realizations enumerated in Table I, using a simple cut and counts statistical technique.

Note that a general relativistic WIMP-nucleon interaction can be expanded in the nonrelativistic EFT operator base of Eq. (1) resulting in a linear combination of the terms listed in Table I. However, the corresponding 90% C.L. exclusion curve cannot be immediately deduced by
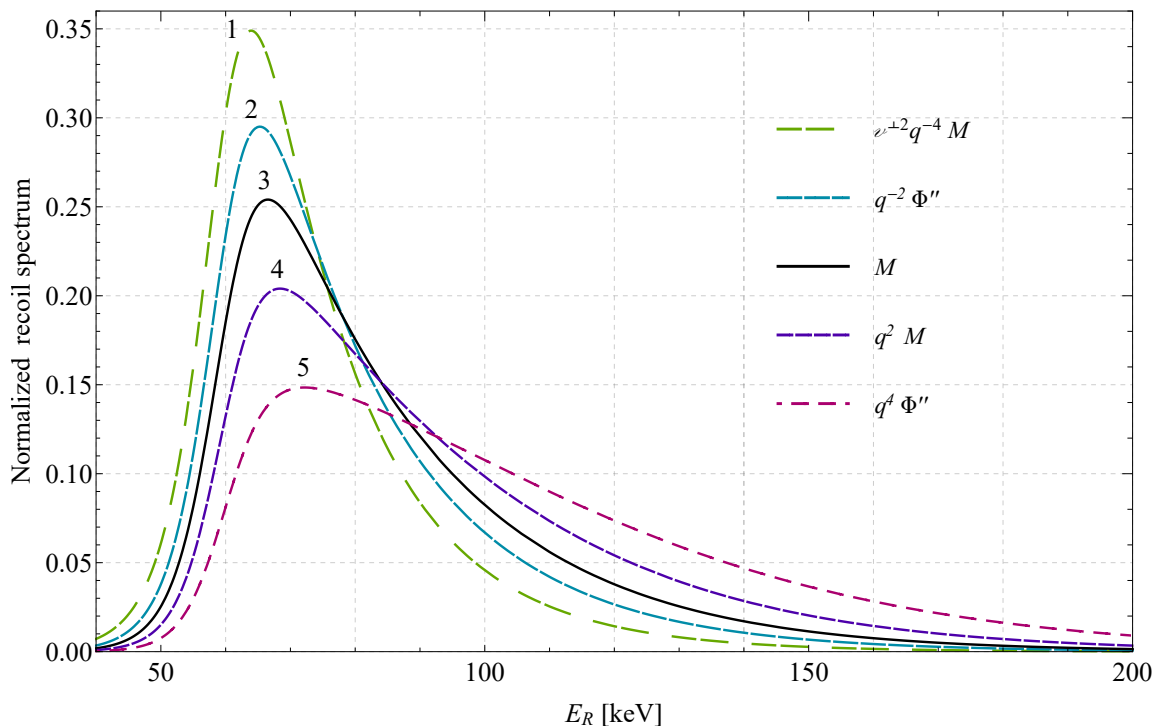
FIG. 1. Expected recoil-energy spectra of argon nuclei in DarkSide-50 from the interaction of 100 MeV/c^2 WIMPs with the SHM velocity distribution for five different EFT operators. Spectra include the acceptance of the detector and are arbitrary normalized. Curve labeled (3) shows the standard spectrum corresponding to the SI operator, i.e., the form factor M in the adopted notation. The other four curves correspond to (1) the nuclear response function M times the the factor $v^{\perp 2} q^{-4}$, (2) Φ'' times q^{-2}, (4) M times the factor q^2, and (5) Φ'' times q^4.

	σ_i (cm^2)	
Model	$M_\chi = 100$ GeV/c^2	$M_\chi = 1000$ GeV/c^2
$q^4 \Phi''$	2.3×10^{-42}	6.0×10^{-42}
$q^2 \Phi''$	1.6×10^{-42}	4.9×10^{-42}
Φ''	1.0×10^{-42}	3.5×10^{-42}
$q^{-2} \Phi''$	6.2×10^{-43}	2.3×10^{-42}
$q^2 M$	1.8×10^{-44}	5.5×10^{-44}
M	1.1×10^{-44}	3.8×10^{-44}
$v^{\perp 2} q^2 M$	1.2×10^{-44}	3.5×10^{-44}
$q^{-2} M$	6.6×10^{-45}	2.5×10^{-44}
$v^{\perp 2} M$	7.4×10^{-45}	2.5×10^{-44}
$v^{\perp 2} q^{-2} M$	4.3×10^{-45}	1.6×10^{-44}
$q^{-4} M$	3.7×10^{-45}	1.5×10^{-44}
$v^{\perp 2} q^{-4} M$	2.4×10^{-45}	8.9×10^{-45}

TABLE II. Values of the cross section parameters σ_i for the 12 EFT terms as defined in Eq. (7) excluded at the 90% C.L. for two values of the WIMP mass.

the individual curves for each NR operator.

There are two groups of curves in Fig. 2: the eight curves at the bottom correspond to the standard spin-independent coherent response function M, and the four curves at the top correspond to the form factor Φ'' and give much weaker limits. This last form factor is related to spin-orbit coupling mainly of the two unpaired neutrons and the two proton holes in ^{40}Ar and it is therefore about a factor $(4/40)^2$ smaller than M. Within each group, the operator proportional to the smaller power
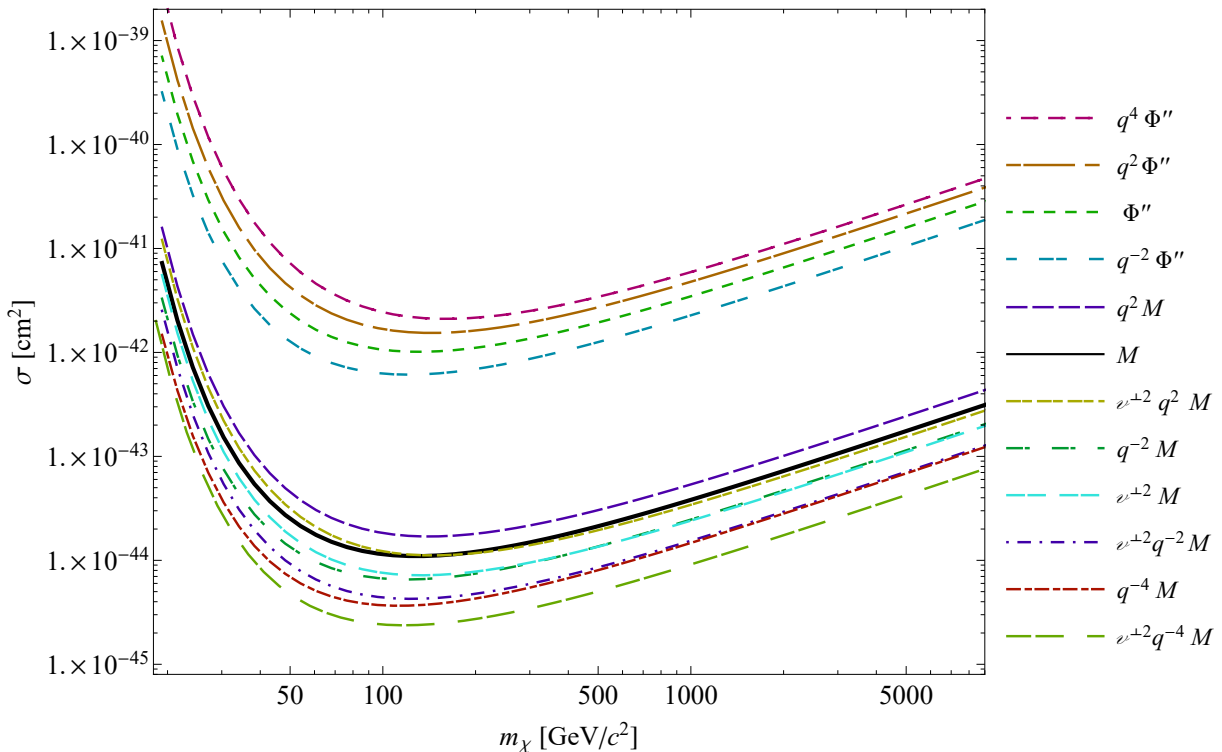
FIG. 2. DarkSide-50 90% C.L. exclusion curves on the cross section parameter σ_i for the 12 EFT terms as defined by Eq. (7). Going from top to bottom, we see a group of four curves that correspond to the nuclear response function Φ'' times q^4, q^2, 1, or q^{-2}; then a group of eight curves corresponding to the nuclear response function M times q^2, 1, $q^2 v^{\perp 2}$, q^{-2}, $v^{\perp 2}$, $q^{-2} v^{\perp 2}$, q^{-4}, or $q^{-4} v^{\perp 2}$. The solid black curve represents the standard spin-independent limit that corresponds to the current limit published in Ref. [25].

of q gets the stronger limit, since the expected rates are higher when lower recoil energies have larger weight. Table II shows the 90% C.L. limits for the 12 cross sections for WIMPs of mass of 100 GeV/c^2 and 1000 GeV/c^2.

CONCLUSIONS

We have reanalyzed the latest DarkSide-50 results with a total exposure of (16660 ± 270) kg d in terms of the 12 leading effective operators naturally appearing in a nonrelativistic expansion. This extended set of operators leads to 90% C.L. upper limits on the effective couplings that parametrize the WIMP-nucleon interaction. These couplings, one of which is the coherent SI standard interaction span many orders of magnitude. Figure 2 shows the experimental constraints as a function of the WIMP mass and in Table II the corresponding numerical values for WIMPs of masses of 100 GeV/c^2 and 1000 GeV/c^2 are highlighted. For instance, for the interaction parametrized only by the operator leading to the nuclear response function M times $q^{-4} v^{\perp 2}$, the DarkSide-50 data yield a 90% confidence limit on the corresponding cross section, as defined in Eq. (7), of 2.4×10^{-45} cm^2 (8.9×10^{-45} cm^2) for a WIMP mass of

100 (1000) GeV/c^2, which is a factor about five more stringent than the standard SI limit. On the contrary, for the interaction parametrized by the Φ'' nuclear function times q^4, the limit on the corresponding cross section is only 2.3×10^{-42} cm^2 (6.0×10^{-42} cm^2) for a 100 (1000) GeV/c^2, more than 2 orders of magnitude larger than the standard SI limit. Different operators also predict different WIMP recoil spectra, as shown in Fig. 1. Thus, different interaction models could be tested if enough WIMP events will be detected in the future. Moreover, the relative importance of the different EFT operators depends on the target nuclei that can have very different response functions. One should be prudent when comparing limits and/or signals from experiments with different targets under the assumption of the simplest interaction model, the SI scalar cross section. The complementarity of experiments using different targets could be crucial for probing the full parameter space.

ACKNOWLEDGMENTS

ᵃ Deceased.

[1] S. M. Faber and J. S. Gallagher, Annu. Rev. Astro. Astrophys. 17, 135 (1979).

[2] D. N. Spergel, Phys. Rev. D 37, 1353 (1988).

[3] D. Clowe et al., Ap. J. 648, L109 (2006).

[4] J. L. Feng, Annu. Rev. Astro. Astrophys. 48, 495 (2010).

[5] A. L. Fitzpatrick, W. Haxton, E. Katz, N. Lubbers, and Y. Xu, ArXiv e-prints (2012), arXiv:1211.2818 [hep-ph].

[6] A. L. Fitzpatrick, W. Haxton, E. Katz, N. Lubbers and Y. Xu, JCAP 1302, 004 (2013) doi:10.1088/1475-7516/2013/02/004 [arXiv:1203.3542 [hep-ph]].

[7] N. Anand, A. L. Fitzpatrick and W. C. Haxton, Phys. Rev. C 89, no. 6, 065501 (2014) doi:10.1103/PhysRevC.89.065501 [arXiv:1308.6288 [hep-ph]].

[8] J.D. Lewin and P. Smith, Astropart. Phys. 6, 87 (1996).

[9] C. Savage, K. Freese, and P. Gondolo, Phys. Rev. D 74, 043531 (2006).

[10] M.C. Smith et al., Mon. Not. Roy. Astron. Soc. 379, 755 (2007).

[11] C. Savage, G. Gelmini, P. Gondolo, and K. Freese, JCAP 0904, 010 (2009).

[12] R. Bernabei et al., Eur. Phys. J. C 67, 39 (2010).

[13] R. Bernabei et al., Universe 4, no. 11, 116 (2018) doi:10.3390/universe4110116 [arXiv:1805.10486 [hep-ex]].

[14] R. Agnese et al. [CDMS Collaboration], Phys. Rev. Lett. 111, no. 25, 251301 (2013) doi:10.1103/PhysRevLett.111.251301 [arXiv:1304.4279 [hep-ex]].

[15] E. Aprile et al. (The XENON100 Collaboration), Phys. Rev. Lett. 109, 181301 (2012).

[16] D. S. Akerib et al. [LUX Collaboration], Phys. Rev. Lett. 118, no. 25, 251302 (2017) doi:10.1103/PhysRevLett.118.251302 [arXiv:1705.03380 [astro-ph.CO]].

[17] X. Cui et al. [PandaX-II Collaboration], Phys. Rev. Lett. 119, no. 18, 181302 (2017) doi:10.1103/PhysRevLett.119.181302 [arXiv:1708.06917 [astro-ph.CO]].

[18] E. Aprile et al. [XENON Collaboration], Phys. Rev. Lett. 121, no. 11, 111302 (2018) doi:10.1103/PhysRevLett.121.111302 [arXiv:1805.12562 [astro-ph.CO]].

[19] K. Schneck et al. [SuperCDMS Collaboration], Phys. Rev. D 91 (2015) no.9, 092004 doi:10.1103/PhysRevD.91.092004 [arXiv:1503.03379 [astro-ph.CO]].

[20] V. Gluscevic, M. I. Gresham, S. D. McDermott, A. H. G. Peter and K. M. Zurek, JCAP 1512 (2015) no.12, 057 doi:10.1088/1475-7516/2015/12/057 [arXiv:1506.04454 [hep-ph]].

[21] M. Cirelli, E. Del Nobile and P. Panci, JCAP 1310 (2013) 019 doi:10.1088/1475-7516/2013/10/019 [arXiv:1307.5955 [hep-ph]].

[22] E. Aprile et al. [XENON Collaboration], Phys. Rev. D 96, no. 4, 042004 (2017) doi:10.1103/PhysRevD.96.042004 [arXiv:1705.02614 [astro-ph.CO]].

[23] J. Xia et al. [PandaX-II Collaboration], arXiv:1807.01936 [hep-ex].

[24] B. A. Dobrescu and I. Mocioiu, JHEP 0611 (2006) 005 doi:10.1088/1126-6708/2006/11/005 [hep-ph/0605342].

[25] P. Agnes et al. [DarkSide Collaboration], Phys. Rev. D 98, no. 10, 102006 (2018) doi:10.1103/PhysRevD.98.102006 [arXiv:1802.07198 [astro-ph.CO]].

[26] W. L. Guo, Z. L. Liang and Y. L. Wu, Nucl. Phys. B 878 (2014) 295 doi:10.1016/j.nuclphysb.2013.11.016 [arXiv:1305.0912 [hep-ph]].

[27] M. Hoferichter, P. Klos, J. Menndez and A. Schwenk, Phys. Rev. D 94, no. 6, 063505 (2016) doi:10.1103/PhysRevD.94.063505 [arXiv:1605.08043 [hep-ph]].

[28] R. Catena and B. Schwabe, "Form factors for dark matter capture by the Sun in effective theories," JCAP 1504, no. 04, 042 (2015) doi:10.1088/1475-7516/2015/04/042 [arXiv:1501.03729 [hep-ph]].

[29] T. Alexander et al. [DarkSide Collaboration], searches," Astropart. Phys. 49 (2013) 44 doi:10.1016/j.astropartphys.2013.08.004 [arXiv:1204.6218 [astro-ph.IM]].

[30] P. Agnes et al. [DarkSide Collaboration], JINST 11 (2016) no.03, P03016 doi:10.1088/1748-0221/11/03/P03016 [arXiv:1512.07896 [physics.ins-det]].

[31] P. Agnes et al. [DarkSide Collaboration], Phys. Rev. D 93, no. 8, 081101 (2016) Addendum: [Phys. Rev. D 95, no. 6, 069901 (2017)] doi:10.1103/PhysRevD.93.081101, 10.1103/PhysRevD.95.069901 [arXiv:1510.00702 [astro-ph.CO]].

[32] P. Agnes et al. [DarkSide Collaboration], JINST 12, no. 12, T12004 (2017) doi:10.1088/1748-0221/12/12/T12004 [arXiv:1611.02750 [physics.ins-det]].

[33] H. Cao et al. [SCENE Collaboration], Phys. Rev. D 91, 092007 (2015) doi:10.1103/PhysRevD.91.092007 [arXiv:1406.4825 [physics.ins-det]].

[34] P. Agnes *et al.*, Phys. Rev. D **97**, no. 11, 112005 (2018) doi:10.1103/PhysRevD.97.112005 [arXiv:1801.06653 [physics.ins-det]].

[35] P. Agnes *et al.* [DarkSide Collaboration], Phys. Rev. Lett. **121**, no. 8, 081307 (2018) doi:10.1103/PhysRevLett.121.081307 [arXiv:1802.06994 [astro-ph.HE]].

[36] P. Agnes *et al.* [DarkSide Collaboration], Nazionali del Gran Sasso," Phys. Lett. B **743** (2015) 456 doi:10.1016/j.physletb.2015.03.012 [arXiv:1410.0653 [astro-ph.CO]].

[37] P. Agnes *et al.* [DarkSide Collaboration], JINST **11**, no. 03, P03016 (2016) doi:10.1088/1748-0221/11/03/P03016 [arXiv:1512.07896 [physics.ins-det]].

[38] P. Agnes *et al.* [DarkSide Collaboration], JINST **11**, no. 12, P12007 (2016) doi:10.1088/1748-0221/11/12/P12007 [arXiv:1606.03316 [physics.ins-det]].

[39] P. Agnes *et al.* [DarkSide Collaboration], JINST **12**, no. 12, P12011 (2017) doi:10.1088/1748-0221/12/12/P12011 [arXiv:1707.09889 [physics.ins-det]].

[40] P. Agnes *et al.* [DarkSide Collaboration], JINST **12**, no. 10, P10015 (2017) doi:10.1088/1748-0221/12/10/P10015 [arXiv:1707.05630 [physics.ins-det]].

[41] D. Acosta-Kane et al., Nucl. Inst. Meth. A **587**, 46 (2008); H. O. Back et al., arXiv:1204.6024v2 (2012); H. O. Back et al., arXiv:1204.6061v2 (2012); J. Xu et al., Astropart. Phys. **66**, 53 (2015).